Supplement of Biogeosciences, 20, 2837–2855, 2023
https://doi.org/10.5194/bg-20-2837-2023-supplement

Biogeosciences Open Access EGU

Supplement of

Simulated methane emissions from Arctic ponds are highly sensitive to warming

Zoé Rehder et al.

Correspondence to: Zoé Rehder (zoe.rehder@mpimet.mpg.de)

Supplement 1: documentation of the MeEP methane module

1.1 Summer fluxes

In ponds, methane (CH_4) is produced in the anoxic bottom sediments when temperatures permit. If the pond is ice-free, this methane evades through three pathways: Diffusion, plant-mediated transport, and ebullition. To model these pathways and the distribution of produced methane between these pathways, we make the following main assumptions:

1. Production and emissions are in equilibrium in each time step and, consequently, the methane concentrations in the water column are stationary. This means that the time-derivatives of the methane concentrations and fluxes are all zero in each time step.

2. There is no lateral mixing of methane between the vegetated part and the open-water part of the pond in summer. Thus, methane transport in both parts of the pond can be treated separately.

3. In summer, the whole water column is well mixed, and the methane concentration throughout the water column is constant.

Following assumption 2, we can model the overgrown and the open-water part of the pond separately. Only for the overgrown fraction plant-mediated transport is considered.

1.1.1 Methane in the sediment

Methane is produced in the sediment, and the production is dependent on the sediment temperature T_b [K] and the base productivity P_0 [mol m^{-3} s^{-1}]. P_0 is a tuning parameter and separately tuned for the overgrown and open-water parts of the ponds (Ström et al., 2003). We assume that most methane is produced at the top of the sediment ($z = 0$ m), and the productivity reduces exponentially further down the sediment ($z > 0$ m) (Stepanenko et al., 2011):

$$P_{CH_4}(z) = P_0 \cdot e^{-az} \cdot q_{10}^{(T_b - 273.15)/T_{10}} \cdot f_{\text{prod}} \qquad [\text{mol m}^{-3}\ \text{s}^{-1}]. \tag{1}$$

q_{10} and T_{10} [C] are constants describing the temperature dependence, while a [m^{-1}] determines how quickly the methane production decreases with sediment depth. Since methane production has been reported to reduce quickly with sediment depth (Knoblauch et al., 2015), we set a to 20 m^{-1} (see Tab. S3). With f_{prod} we take substrate availability into account. This dimensionless factor is based on Walter et al. (2001) and represents both the productivity of the plants and an estimate for the litter fall: We assume that carbon availability is correlated with the net primary productivity (NPP), and that net primary productivity is roughly half of the gross primary productivity (GPP). Since the methanogens do not use all the substrate within the same time step, we apply a running average on NPP with a window length of one month split methane production into a part dependent on NPP (75%) and into a base productivity (25%) based on findings by Bouchard et al. (2015) and Dean et al. (2020). For the open-water part of the pond, we additionally assume that the carbon availability decreases with the open-water fraction and multiply the NPP-dependent term with $\tanh(A_v/A_o)$, where A_v is the overgrown area of the pond, and A_o is the area of the open-water fraction.

Since the fraction of the sediment where methane is produced is shallow, we can assume a constant temperature in the sediment layer and integrate Eq. 1 from the top of the sediment ($z = 0$ m) to the bottom of the unfrozen sediment ($z = h_s$) resulting in

$$P_{CH_4} = \frac{P_0}{a} \cdot q_{10}^{(T_b - 273.15)/T_{10}} \cdot (1 - e^{-ah_s}) \cdot f_{\text{prod}} \qquad [\text{mol m}^{-2}\ \text{s}^{-1}]. \tag{2}$$

We use Eq. 2 to simulate the production of methane in the sediment when the temperature in the topsoil exceeds the freezing point. As soon as the sediment freezes, we set the methane production to zero.

The methane fluxes out of the sediment reach their maximum when the methane concentration in the sediment is as high as physically possible. The methane gradient between the sediment and the water column is maximal at this concentration. The saturation concentration is reached when methane starts to gas out and form bubbles. Bubbles forming in the sediment can contain any gas present in the sediment. The most abundant gas in air is nitrogen, so it is also the most abundant gas in the sediment, and, apart from methane, the main constituents of bubbles in the sediment (Walter et al., 2008). Thus, we approximate that the bubbles contain only methane and nitrogen to derive the saturation concentration. Under this assumption, the concentration of methane is limited by the hydro-static pressure p_h (Pa) and the partial pressure of nitrogen (N_2) (Stepanenko et al., 2011; Bazhin, 2001). To compute the saturation concentration of methane, we assume that N_2 decays exponentially in the sediment and is in equilibrium with the atmosphere in the water column ($c(N_2, z) = c(N_2)_{eq} \cdot e^{-\lambda_{N_2}(z-h_s)}$ [mol m^{-3}]). $c(N_2)_{eq}$ can be computed according to Henry's law, and we define $H_b^{N_2}$ as

the temperature-dependent Henry constant for N_2 at sediment temperatures. $H_b^{CH_4}$ [mol m^{-1} Pa^{-1}] signifies the equivalent Henry constant for methane (Sander, 2015). We compute the temperature-dependent Henry constant as follows:

$$H^{\mathbf{gas}} = H_0^{\mathbf{gas}} e^{\tau(1/T - 1/T_0)} \qquad [\text{mol m}^{-3}\ \text{Pa}^{-1}]. \tag{3}$$

Another quantity driving the saturation concentration, the hydrostatic pressure is computed as the sum of the air pressure p_a and the pressure exerted by the water column,

$$p_h = p_a + (H \cdot \rho_{aq} \cdot g) \qquad [\text{Pa}]. \tag{4}$$

Further, the saturation pressure depends on the porosity of the sediment ϕ [m^3 m^{-3}], which is set based on measurement data (Helbig et al., 2013; Zubrzycki et al., 2013) and a dimensionless threshold γ. γ is introduced as a correction factor to account for the shape of the bubbles. Henry's law was measured over flat surfaces, but bubbles are spherical (Stepanenko et al., 2011). Due to large uncertainty regarding the true value of γ, γ is tuned. Combining Eq. 3 and Eq. 4 with γ and ϕ, we arrive at the following equation for the saturation concentration:

$$c(CH_4)_b^{\text{sat}} = \phi \cdot H_b^{CH_4} \cdot \gamma \cdot \left(p_h - \frac{c(N_2)_{eq}}{H_b^{N_2}} \cdot e^{\frac{-\lambda_{N_2} \cdot h_s}{2}} \right) \qquad [\text{mol m}^{-3}]. \tag{5}$$

Once this concentration is reached, all additional methane produced in the sediment will change from dissolved to gaseous. Consequently, the concentration in the sediment will not rise further no matter how much additional methane is produced.

1.1.2 Plant-mediated transport

Plants can be very efficient in transmitting methane from the sediment to the atmosphere bypassing the water column. If plants are present, plant-mediated transport is often the dominating pathway (Andresen et al., 2017). Thus, out of the three possible pathways, we evaluate the plant-mediated transport first using the approach by Walter et al. (1996). Initially, we compute the rate Q_{plant} with which methane can leave the root zone through the plants as

$$Q_{\text{plant}} = d_{\text{veg}} \cdot t_{\text{veg}} \cdot r \cdot f_{\text{growth}} \cdot h_s \cdot c(CH_4)_b^{\text{sat}} \qquad [\text{mol m}^{-2}\ \text{s}^{-1}]. \tag{6}$$

d_{veg} is a dimensionless factor for the density of the plants, which we set to globally to 0.1 due to lack of data. t_{veg} is another dimensionless factor describing how well the plants conduct methane and is set to 10 based on Walter et al. (2001). r is a rate constant of 0.01 h^{-1} $= 2.7 \cdot 10^{-6}$ s^{-1}. f_{growth} is a dimensionless measure of the plant-growth, varies between zero and four and is based on the leaf-area index. Andresen et al. (2017) found a good agreement between leaf-area index and plant-biomass for the dominant species in Arcitc ponds (*Arctophila fulva* and *Carex aquatilis*). h_s [m] is the depth of the unfrozen sediment, with a maximum thickness of 0.2 m, because deeper sediments produce only very little methane (Knoblauch et al., 2015; Joabsson and Christensen, 2001). Since the plant stems also transport oxygen into the rooting zone, we assume a fixed fraction of the plant-mediated methane to be oxidized ($f_{\text{ox}} = 0.2$) reducing the methane flux from plants F_{plant}. The value 0.2 is an conservative estimate based on the work of Turner et al. (2020) and Ström et al. (2005), who measured the oxidation rates of the plant species dominating our study region. The plant-mediated flux then is defines as

$$F_{\text{plant}} = (1 - f_{\text{ox}}) \cdot \min\{Q_{\text{plant}}, P_{CH_4}\} \qquad [\text{mol m}^{-2}\ \text{s}^{-1}]. \tag{7}$$

Since plants, if present, are the most efficient pathway for methane removal from the sediment, we assume that all methane that can be emitted through plants, is emitted through plants. Thus, only excess methane which cannot be emitted through plants is available for the other pathways.

1.1.3 Diffusion

Since ponds are shallow and well mixed, we assume that the methane concentration in the pond $c(CH_4)_{aq}$ [mol m^{-3}] are constant throughout the water column. This allows us to formulate the following balance of the flux between sediment and water column F_b^{diff} [mol m^{-2} s^{-1}], the flux between water surface and atmosphere F_{diff} [mol m^{-2} s^{-1}], and the oxidation in the water column F_{ox} [mol m^{-2} s^{-1}]:

$$F_b^{\text{diff}} - F_{\text{diff}} - F_{ox} = 0. \tag{8}$$

Now, we take a look at each of these three fluxes before we subsitute formulations for each back into the balance above.

Sediment-Water Interface We compute the diffusion from the sediment into the water column according to Fick's law and assuming that the methane concentration in the sediment equals the saturation concentration $c(CH_4)_b^{\text{sat}}$ (Eq. 5),

$$F_b^{\text{diff}} = D_{\text{soil}} \frac{c(CH_4)_b^{\text{sat}} - c(CH_4)_{aq}}{0.5 \cdot h_s} \qquad [\text{mol m}^{-2}\ \text{s}^{-1}], \tag{9}$$

with the diffusion coefficient D_{soil}. This coefficient is computed following Sabrekov et al. (2017) as a combination of liquid and gaseous diffusion as

$$D_{\text{soil}} = (\phi - \epsilon_a) D_{\text{aq}} + \frac{\epsilon_a \cdot D_{\text{gas}}}{H_b^{CH_4} \cdot R \cdot T_b} \qquad [\text{m}^2\ \text{s}^{-1}]. \tag{10}$$

ϵ_a is the gas-filled porosity of the soil. Since this parameter is ill-constrained, it was used as a tuning parameter. R is the ideal gas constant, and the liquid and gaseous diffusion coefficients (D_{aq} and D_{gas}, respectively) are computed as

$$D_{\text{aq}} = \tau \cdot (\phi - \epsilon_a) \cdot D_{\text{aq}}^0 \cdot ((T_b - 0.15)/298)^{1.82} \qquad [\text{m}^2\ \text{s}^{-1}], \tag{11}$$

$$D_{\text{gas}} = D_{\text{gas}}^0 \cdot \epsilon_a^{3.3}/\phi^2 \cdot ((T_b - 0.15)/273)^{1.82} \qquad [\text{m}^2\ \text{s}^{-1}]. \tag{12}$$

τ is the dimensionless tortuosity coefficient, T_b [K] is the temperature of the upper sediment, D_{aq}^0 [m^2 s^{-1}] and D_{gas}^0 [m^2 s^{-1}] are reference values for the diffusivity of methane and set according to Arah and Stephen (1998).

Water-Air Interface We infer the diffusion from the water column to the atmosphere using the gradient between water and air analogously to the sediment-water interface,

$$F_{\text{diff}} = k_p (c(CH_4)_{\text{aq}} - c(CH_4)_{aq}^{\text{eq}}) \qquad [\text{mol m}^{-2}\ \text{s}^{-1}]. \tag{13}$$

$c(CH_4)_{aq}^{\text{eq}}$ [mol m^{-3}] represents the methane concentration in equilibrium with the atmosphere, and k_p [m s^{-1}] is the piston velocity, or gas-exchange coefficient. $c(CH_4)_{aq}^{\text{eq}}$ is computed using the ideal gas law and Henry's law as

$$c(CH_4)_{aq}^{\text{eq}} = f_{CH_4}^{atm} \cdot p_a \cdot H_{aq}^{CH_4}. \tag{14}$$

$f_{CH_4}^{atm}$ denotes the fraction of methane in air, $H_{aq}^{CH_4}$ [mol m^{-1} Pa^{-1}] is the temperature-dependent Henry's constant for methane in the water column using the mixed-layer temperature (Sabrekov et al., 2017).

For k_p, we follow the parameterization by Heiskanen et al. (2014),

$$k_p = \frac{\sqrt{(c_1^{\text{piston}} \cdot u)^2 + (c_2^{\text{piston}} \cdot w_{dd})^2}}{\sqrt{S}} \qquad [\text{m s}^{-1}]. \tag{15}$$

c_1^{piston} and c_2^{piston} are dimensionless constants, which were tuned to data of lakes in the original paper. u [m s^{-1}] is the wind speed, which is a forcing variable, and w_{dd} [m s^{-1}] is the Deardoff velocity computed using FLake. Lastly, S is the dimensionless Schmidt number, which we compute following Wanninkhof (2014, 1992),

$$S = c_1^S + c_2^S \cdot T_{\text{ml}} + c_3^S \cdot T_{\text{ml}}^2 + c_4^S \cdot T_{\text{ml}}^3 + c_5^S \cdot T_{\text{ml}}^4. \tag{16}$$

c_1^S to c_5^S are empirically determined constants, T_{ml} [K] is the mixed-layer temperature provided by FLake.

Oxidation in the water column For F_{ox} we assume that the water oxygen concentration is in equilibrium with the atmosphere and compute $c(O_2)_{\text{aq}}$ in the same manner as $c(CH_4)_{aq}^{\text{eq}}$,

$$c(O_2)_{\text{aq}} = f_{O_2}^{atm} \cdot p_a \cdot H_{aq}^{O_2} \qquad [\text{mol m}^{-3}]. \tag{17}$$

Then we use the Michaelis-Menthen relation to compute the oxidation,

$$F_{ox} = V_{\max} \cdot H \ \frac{c(O_2)_{\text{aq}}}{k_{O_2} + c(O_2)_{\text{aq}}} \ \frac{c(CH_4)_{\text{aq}}}{k_{CH_4} + c(CH_4)_{\text{aq}}} \qquad [\text{mol m}^{-2}\ \text{s}^{-1}]. \tag{18}$$

$V_{\max}$ [mol m^{-3} s^{-1}], k_{CH_4} [mol m^{-3}] and k_{O_2} [mol m^{-3}] are constants and set based on a study by Martinez-Cruz et al. (2015) focusing on Alaskan lakes.

Methane concentration in the mixed layer We can now substitute the fluxes (eq. (9), (13), and (18)) into the balance (eq. 8). This leads to an quadratic equation of $c(CH_4)_{\text{aq}}$ which we can solve analytically and arrive at the following expression for $c(CH_4)_{\text{aq}}$:

$$c(CH_4)_{\text{aq}} = \frac{c + \sqrt{c^2 + 4k_{CH_4} \cdot a \cdot b)}}{2b} \qquad [\text{mol m}^{-3}], \tag{19}$$

$$a = \frac{1}{H \cdot k_{ox}} \left(\frac{D_{\text{soil}} \cdot c(CH_4)^{\text{eq}}_{aq}}{0.5 h_s} + k_p \cdot c(CH_4)^{\text{sat}}_{b} \right) \qquad [\text{ - }], \tag{20}$$

$$b = \frac{1}{H \cdot k_{ox}} \left(\frac{D_{\text{soil}}}{0.5 h_s} + k_p \right) \qquad [\text{m}^3\text{mol}^{-1}], \tag{21}$$

$$c = a - k_{CH_4} \cdot b - 1 \qquad [\text{ - }]. \tag{22}$$

k_{ox} denote the part of the Michaelis-Menten relation which does not depend on CH_4,

$$k_{ox} = V_{\max} \frac{c(O_2)_{\text{aq}}}{k_{O_2} + c(O_2)_{\text{aq}}} \qquad [\text{mol m}^{-3}\ \text{s}^{-1}]. \tag{23}$$

Once we obtained $c(CH_4)_{\text{aq}}$, we can compute the flux from the sediment and compare this potential diffusive flux with the methane production to compute the diffusive flux from the sediment into the waterbody (Eq. 9) as

$$F^{\text{diff}}_b = \min\{P_{CH_4} - F_{\text{plant}}, F^{\text{diff}}_b\}. \tag{24}$$

In case the F^{diff}_b computed using Eq. 9 is larger than the remaining methane in the atmosphere ($P_{CH_4} - F_{\text{plant}}$), we solve Eq. 8 again for $c(CH_4)_{\text{aq}}$ again, this time with the boundary condition $F^{\text{diff}}_b = P_{CH_4} - F_{\text{plant}}$. This, then, results in

$$c(CH_4)_{\text{aq}} = \frac{a + \sqrt{a^2 + b}}{2k_p} \qquad [\text{mol m}^{-3}], \tag{25}$$

$$a = k_p(c(CH_4)^{\text{eq}}_{aq} - k_{CH_4}) - H \cdot k_{ox} + F^{\text{diff}}_b \qquad [\text{mol m}^{-2}\ \text{s}^{-1}], \tag{26}$$

$$b = 4k_p \cdot k_{CH_4}(k_p \cdot c(CH_4)^{\text{eq}}_{aq} + F^{\text{diff}}_b) \qquad [\text{mol}^2\text{m}^{-4}\ \text{s}^{-2}]. \tag{27}$$

Finally, we can substitute either the result of eq. 19 or eq. 25 into eq. 13 and obtain the diffusive flux from the pond to the atmosphere.

1.1.4 Ebullition

The third and last pathway of methane from the sediment to the atmosphere is ebullition. We assumed that plant-mediated transport is the fastest pathway of methane and computed that flux first. With the methane left in the sediment ($P_{CH_4} - F_{\text{plant}}$), we computed the diffusive flux between water and atmosphere F_{diff} and the diffusive flux between sediment and water F^{diff}_b. Since we assume that production and emission are in equilibrium, all the methane that is still left in the sediment and not emitted through diffusion or plants is emitted through ebullition,

$$F_{\text{ebul}} = P_{CH_4} - F_{\text{plant}} - F^{\text{diff}}_b \qquad [\text{mol m}^{-2}\ \text{s}^{-1}]. \tag{28}$$

1.2 Winter fluxes

1.2.1 Ice-covered ponds

Once ice has formed on the pond, we assume there is no gas exchange between water and atmosphere, so all fluxes to the atmosphere are set to zero. This means that there is also no plant-mediated transport, which was the mechanism setting the overgrown part of the pond apart from the open-water part. So instead of treating the overgrown and open-water fractions of the pond separately, we can simulate them together in winter. We merge the two parts weighted by their area fraction for the methane production in the sediment and methane concentration in the water column. We take the deeper water column height as the water column height for the merged computation. As the ice layer grows, we assume that all soluble gases that were dissolved in the freshly frozen water are expelled into the underlying water column. In the same manner methane and oxygen concentrations in water are diluted when ice melts,

$$c(\mathbf{gas})(t) = \frac{H_{aq} + \Delta_{\text{ice}}}{H_{aq}}\ c(\mathbf{gas})(t-1), \tag{29}$$

where **gas** stands for either oxygen or methane, and H_{aq} the height of the unfrozen water column. t is the time step and $\Delta_{\text{ice}} = h_{\text{ice}}(t) - h_{\text{ice}}(t-1)$ is the change in ice thickness, with a positive sign indicating ice growth.

Since the pond cools down from the top, sediment temperatures are still above freezing when ice forms in fall. Thus, methane is still produced in fall until sediment temperatures drop to zero, and there is still a methane flux from the sediment into the water column. Thus, all the methane produced in a time step (see eq. (2)) is added to the water column,

$$c(CH_4)_{\text{aq}}(t) = c(CH_4)_{\text{aq}}(t) + P_{CH_4} \frac{t_s}{H_{aq}} \qquad [\text{mol m}^{-3}], \tag{30}$$

with t_s being the time step length. Since the methane cannot be emitted to the atmosphere, it accumulates in the water column where a part of the methane is oxidized with the remaining dissolved oxygen. If the methane concentration exceeds a threshold $c(CH_4)^{\text{sat}}_{aq}$, it changes its state from dissolved to gaseous, equivalently to the processes in the sediment. The position where the bubbles are most likely to form is directly under the ice, because the hydrostatic pressure is lowest there. We compute the saturation pressure analogously to the equilibrium pressure in summer (eq. 14), but instead of using the partial pressure of methane, we use the hydrostatic pressure

$$p_{\text{hyd}} = p_a + \rho_{\text{ice}}\ g\ h_{\text{ice}} \qquad [\text{Pa}]. \tag{31}$$

Using Henry's law, we compute the saturation pressure of methane under ice as

$$c(CH_4)^{\text{sat}}_{aq} = p_{\text{hyd}} \cdot H^{CH_4}_{aq} \qquad [\text{mol m}^{-3}]. \tag{32}$$

We assume that only the dissolved methane reacts with the oxygen in the water and introduce a storage term S_{CH_4} [mol m^{-2}] for gaseous methane under ice. If the methane concentration in the water column exceeds $c(CH_4)^{\text{sat}}_{aq}$, methane gasses out until $c(CH_4)_{aq} = c(CH_4)^{\text{sat}}_{aq}$.

After balancing S_{CH_4} and $c(CH_4)_{aq}$, we determine how much methane is oxidized in the current time step. To do so, we need to compute the concentration of oxygen under ice, which we prescribe (Huang et al., 2021) as

$$c(O_2)(t) = \max\{0.0, c(O_2)(t-1) - 1.447 \cdot 10^{-7} \cdot t_s\} \qquad [\text{mol m}^{-3}]. \tag{33}$$

We solve the full Michaelis-Menten equation in each time step to estimate how much methane oxidised,

$$\Delta_{ox} = V_{\max} \frac{c(O_2)}{k_{O_2} + c(O_2)} \frac{c(CH_4)_{\text{aq}}}{k_{CH_4} + c(CH_4)_{\text{aq}}} \cdot t_s \qquad [\text{mol m}^{-3}], \tag{34}$$

and reduce methane and the oxygen concentrations in the water accordingly,

$$c(CH_4)_{\text{aq}} = c(CH_4)_{\text{aq}} - \min\{\Delta_{ox},\ c(CH_4)_{\text{aq}},\ c(O_2)/2\}, \tag{35}$$

$$c(O_2)_{\text{aq}} = c(O_2)_{\text{aq}} - 2 \cdot \min\{\Delta_{ox},\ c(CH_4)_{\text{aq}},\ c(O_2)/2\}. \tag{36}$$

Next, we balance S_{CH_4} and $c(CH_4)_{\text{aq}}$ again.

In case the whole water column is frozen, all produced methane is directly added to the storage term S_{CH_4}

1.2.2 Spring flush

Once the ice on the pond has melted, we emit the methane accumulated under the ice to the atmosphere. Since we assume an equilibrium between emission and production of methane in the open-water season, we emit all the accumulated methane in the first time step of open water. All the methane stored in gas-form S_{CH_4} is immediately released through ebullition. Furthermore, we emit the methane, which was dissolved in the water and led to elevated dissolved methane concentration, compared to the open-water case. This dissolved methane is added to the diffusive flux,

$$F_{\text{diff}} = F_{\text{diff}} + \frac{H_{\text{aq}}}{t_s}(c(CH_4)_{\text{aq}}(t-1) - c(CH_4)_{\text{aq}}(t)) \qquad [\text{mol m}^{-2}\ \text{s}^{-1}]. \tag{37}$$

Table S1: Input variables for the methane module of MeEP

Name	Unit	Description	Source
H	m	Mean water depth of open-water and overgrown pond fraction	Hydrology module
A	m^2	Mean area of open-water and overgrown pond fraction	Hydrology module
h_s	m	Thickness of unfrozen bottom sediment layer	Soil module
w_{dd}	m s^{-1}	Convective Deardorff velocity scale in the mixed layer	Flake
u^*	m s^{-1}	Friction velocity scale in the mixed layer	Flake
p_a	Pa	Atmospheric pressure at the surface	ERA-5
T_{ml}	K	Mixed-layer temperature	Flake
T_b	K	Sediment temperature	Soil module
t	s	Time-step length	User choice
h_{ice}	m	Thickness of ice	Flake
Δ_{ice}	m	Change in hice since last time step	Flake
$c(CH_4)_{\mathrm{aq}}$	mol m^{-3}	Methane concentration in the mixed layer of prior time step	Methane module
$c(0_2)_{\mathrm{aq}}$	mol m^{-3}	Oxygen concentration in the mixed layer of prior time step	Methane module
S_{CH_4}	mol m^{-2}	Methane stored under ice in winter	Methane module
ρ	-	Porosity of the sediment	User choice
f_{growth}	-	Approximation of plant growth using the leaf-area index	MODIS
f_{prod}	mol m^{-2}	Net primary production and litter fall approximation	MODIS

Table S2: Tuning parameters for the methane module of MeEP

Name	Values	Unit	Description
P_0^{veg}	0.44	μmol m^{-3} s^{-1}	base productivity in vegetated pond fraction
P_0^{ow}	0.11	μmol m^{-3} s^{-1}	base productivity in vegetated pond fraction
γ	0.26	-	bubble-shape correction factor
ϵ_a	0.046	m^3 m^{-3}	gas-filled porosity of sediment

Table S3: Constants used in the methane module of MeEP

Name	Value	Unit	Description	Equation
a	20	m^{-1}	depth dep. of CH_4 production	1,2
T_{10}	10	°C	reference temp.	1,2
q_{10}	2	-	temp. dep. of CH_4 production	1,2
λ_{N_2}	5	-	depth dep. of N_2 sediment conc.	5
$H_0^{CH_4}$	$1.4 \cdot 10^{-5}$	mol m^{-3} Pa^{-1}	Henry's const. for CH_4	3
$H_0^{O_2}$	$1.3 \cdot 10^{-5}$	mol m^{-3} Pa^{-1}	Henry's const. for O_2	3
$H_0^{N_2}$	$6.4 \cdot 10^{-6}$	mol m^{-3} Pa^{-1}	Henry's const. for N_2	3
$\tau_0^{CH_4}$	1600	K	temp. dep. of Henry's const. for CH_4	3
$\tau_0^{O_2}$	1500	K	temp. dep. of Henry's const. for O_2	3
$\tau_0^{N_2}$	1300	K	temp. dep. of Henry's const. for N_2	3
T_0	25	°C	reference temp.	3
ρ_{aq}	1000	kg m^{-3}	water density	4
g	9.91	m s^{-1}	gravitational acceleration	4, 30
d_{veg}	0.1	-	density of plants	6
t_{veg}	10	-	gas-conducting properties of plants	6
r	$2.7 \cdot 10^{-6}$	s^{-1}	rate const.	6
f_{ox}	0.2	-	oxidised fraction of Q_{plant}	7
R	8.3144598	m^3 Pa K^{-1} mol^{-1}	ideal gas const.	11
τ	0.66	-	tortuosity coeff.	11
D_{aq}^0	$1.5 \cdot 10^{-9}$	m^2 s^{-1}	CH_4 diff. coeff. in the water at 25 °C	11
D_{gas}^0	$1.889 \cdot 10^{-5}$	m^2 s^{-1}	CH_4 diff. coeff. in the air at 0 °C	12
$f_{CH_4}^{atm}$	$1.9499 \cdot 10^{-9}$	-	fraction of CH_4 in atmosphere	15
$f_{N_2}^{atm}$	0.496	-	fraction of N_2 in atmosphere	5
$f_{O_2}^{atm}$	0.19	-	fraction O_2 in atmosphere	18
c_1^{piston}	0.00015	-	weight of wind speed	15
c_2^{piston}	0.07	-	weight of Deardoff velocity	15
c_1^S	1909.4	-	empirical const. for Schmidt num.	17
c_2^S	-120.78	$°C^{-1}$	empirical const. for Schmidt num.	17
c_3^S	4.1555	$°C^{-2}$	empirical const. for Schmidt num.	17
c_4^S	-0.080578	$°C^{-3}$	empirical const. for Schmidt num.	17
c_5^S	0.00065777	$°C^{-4}$	empirical const. for Schmidt num.	17
k_{CH_4}	0.006875	mol m^{-3}	half-saturation const. of CH_4	19,20,23, 35
k_{O_2}	0.0195	mol m^{-3}	half-saturation const. of O_2	19,24, 35
V_{max}	$1.412 \cdot 10^{-7}$	mol m^{-3} s^{-1}	maximum methane oxidation rate	19,24
ρ_{ice}	920	kg m^{-3}	ice density	30
t_s	3600	s	model time-step length	33,35, 38

coeff, coefficient; conc, concentration; const, constant; dep, dependence; diff, diffusion; num, number; temp, temperature.

Supplement 2: documentation of the MeEP hydrology module

In the hydrology module, we compute water-table dynamics throughout the year. To cater to the separation of the open-water and overgrown parts of the pond in the methane module, we set a fraction of the pond to be overgrown and a fraction to be open water based on a maximum water depths for plants. In other words, we assume that vascular plants grow in the shallow parts of the ponds, up to a default depths of 0.5 m. The depths can be set at the beginning of each model run. Any deeper part of a pond consists of open water. The module computes the mean depths of each fraction as well as the area they cover on the premise that the ponds are circular and the cross-section of an isosceles trapezoid (Fig. S1). After the pond has been divided into the

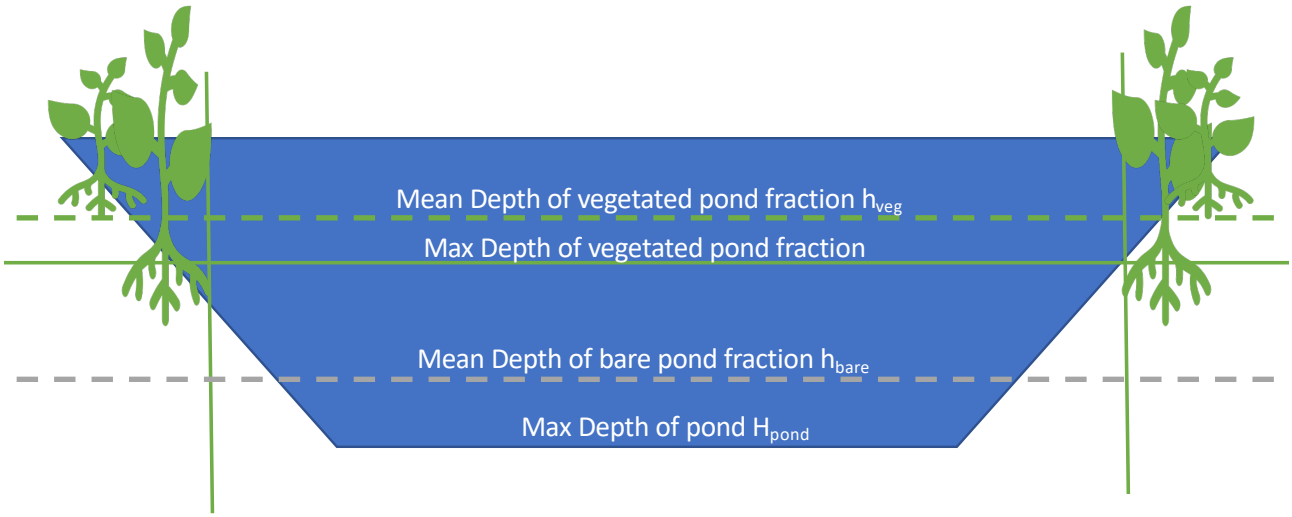

Figure S1: The pond cross-section is assumed to have the shape of an isosceles trapezoid. Plants only grow up to a specific depth (maximum depth of the vegetated pond fraction). For the physical pond model FLake, the maximum depth of the pond is used H_{pond}, which the methane module distinguishes between the vegetated and the open-water part of the pond.

open-water and vegetated parts during initialization, the diameter of the open-water fraction of the pond is kept constant throughout the whole simulation.

2.3 Initialization

To initialize a pond, the user has to set the angle of the rim α (see Fig. S1), the initial depth H_{aq} [m] and the area of the pond. The maximum depth of the pond, before water would overflow, is set to $\text{depth}_{max} = H_{aq} + 0.1$ m. The maximum depth at which plants can grow h_{veg} can be adjusted and has a default of 0.5 m. With h_{veg} [m] the area A [m^2] of the pond is split between an open-water part A_o [m^2] and a vegetated part A_v [m^2]. If H_{aq} is smaller than 0.5 m, the whole pond is vegetated ($A_v = A$ and $A_o = 0$ m^2). Otherwise, we compute the

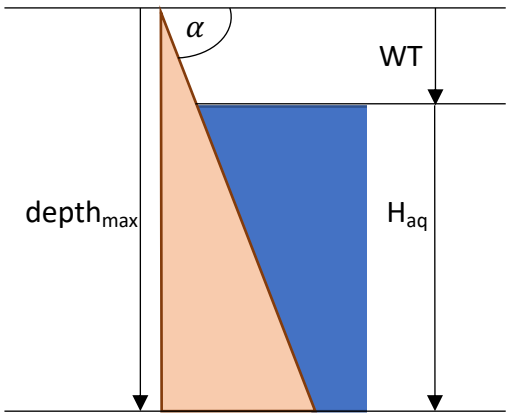

Figure S2: The water table is measured from the highest point of the rim. If the water table is zero, the water depths reaches it's maximum.

area of the open-water part using the assumption that the ponds are circular. The width of the vegetated outer circle R_v [m] can be inferred from α and h_{veg},

$$R_v = \frac{h_{\text{veg}}}{\tan(\alpha)} \qquad [\text{m}]. \tag{38}$$

Then, we subtract R_v from the radius of the whole pond which gives us the radius of the open-water area. With the radii we compute the areas as

$$R = \sqrt{\frac{A}{\pi}} \qquad [\text{m}], \tag{39}$$

$$A_o = \pi \left(R - R_v\right)^2 \qquad [\text{m}^2], \tag{40}$$

$$A_v = A - A_o \qquad [\text{m}^2], \tag{41}$$

where R is the radius of the whole pond. To compute the mean depth of the open-water and the vegetated part of the pond, we compute the volumes of the flat middle part of the pond, and the part of the pond where the water depth increases. The middle part has the shape of a cylinder and can be determined as

$$R_{mid} = R - \frac{H_{aq}}{\tan(\alpha)} \qquad [\text{m}], \tag{42}$$

$$V_{mid} = \pi \cdot R_{mid}^2 \cdot H_{aq} \qquad [\text{m}^3]. \tag{43}$$

$$\tag{44}$$

The outer part can be computed as the volume of a truncated cone minus V_{mid},

$$V_{\text{edge}} = \pi \frac{\tan(\alpha)}{3} (R^3 - 3R \cdot R_{mid}^2 + 2R_{mid}^3) \qquad [\text{m}^3]. \tag{45}$$

We can then compute the volume of the vegetated pond fraction, either as the whole volume of the pond, or as another hollow, truncated cone,

$$V_v[\text{m}^3] = \begin{cases} V_{\text{edge}} + V_{\text{mid}}, & h_{\text{veg}} \leq H_{aq} \\ \pi \frac{\tan(\alpha)}{3} (R^3 - 3RR_o^2 + 2R_o^3), & \text{else,} \end{cases} \tag{46}$$

with $V_o = R - R_v$ the radius of the open-water part of the pond. All the leftover volume of the pond is then attributed to the open-water part.

Finally, we can compute the mean depths of the pond fractions,

$$\overline{h_{o/v}} = \frac{V_{o/v}}{A_{o/v}} \qquad [\text{m}]. \tag{47}$$

2.3.1 Polygonal tundra of Samoylov Island

As an example study site, the ponds can be constructed to represent the three pond types of the polygonal tundra of Samoylov Island. We use a landcover classification to determine the average size of the respective pond type as well as their average vegetated fraction and use the ratio between the open-water and overgrown fraction of the ponds to infer α. For pond depths, we use the averages of measurements done by Rehder et al. (2021). The results are listed in table S4.

Table S4: Input values to initialize typical ponds of the polygonal tundra in the Lena River Delta.

Pond type	Mean area $[\text{m}^2]$	Depth [m]	α [RAD]
polygonal-center pond	89	0.6	0.3
ice-wedge pond	276	0.8	0.2
merged polygonal pond	2682	1.2	0.055

2.4 Water table dynamics

At the beginning of each time step, we add precipitation and evaporation to the water table,

$$WT(t+1) = WT(t) - P + E \qquad [\text{m}]. \tag{48}$$

If this leads to an overflow of the pond, we first compute the surface runoff, Q_s, following Gao et al. (2010),

$$Q_s = \min\{\Delta_z, 5.67\frac{1}{\text{s}}\Delta_z^{3/2}\frac{t_s}{\sqrt{A}}\} \qquad [\text{m}], \tag{49}$$

where $\Delta_z = -WT(t+1)$ represents the height of the water over the theoretical maximum height. If the water table closer to the surface than the thaw depths of the surrounding tundra ($WT(t+1) < TD$), water also runs off below ground. This below-ground runoff Q_b is computed based on Darcy's law as

$$Q_b = KA_c\frac{\Delta_z}{\Delta_x}t_s \qquad [\text{m}]. \tag{50}$$

K [m s^{-1}] indicates the hydraulic conductivity, A_c [m^2] is the area through which the water flows. Δ_x is the distance the water flows through in the porous medium, set to 2m as a characteristic width of a polygonal rim. Δ_z [m] is the height of the water flow and here refers to $TD - WT(t+1)$, where TD is the thaw depth.

K was computed based on measurements by Helbig et al. (2013). They measured the hydrological conductivity on Samoylov Island, Lena River Delta, at different sites. Using the mean of all their measurements, we parameterized an average depth profile of the hydraulic conductivity. With this profile, we compute the hydrological conductivity between TD and $WT(t+1)$ and use the mean K of this profile for further computations,

$$N = \left\lceil \frac{\Delta_z}{0.002\text{m}} \right\rceil, \tag{51}$$

$$z(n) = WT(t+1) + 0.002\text{m} \cdot n, \quad n = 0...N, \tag{52}$$

$$K = \frac{1}{N}\sum_{n=0}^{N} 2.5 \cdot 10^{-4}\frac{\text{m}}{\text{s}}\left(1 + \tanh\left(\frac{0.052\text{m} - z(n)}{0.023\text{m}}\right)\right). \tag{53}$$

Then, we compute A_c as the lateral surface of a cylinder,

$$A_c = 2\Delta_z \cdot \sqrt{\pi \cdot A} \qquad [\text{m}^2]. \tag{54}$$

Finally, the water table is adjusted for the total runoff,

$$WT(t+1) = WT(t+1) + Q_s + Q_b \qquad [\text{m}]. \tag{55}$$

2.5 Recalculating mean water depths

With water table changes, the mean water depth of the overgrown and open-water fraction of the pond change as well as the pond area. Since we account for the inclination of the shoreline, the mean water depth does not necessarily change proportionally to the water table. So we recalculate the mean water depth for both parts of the pond. The radius of the pond changes by

$$\Delta_R = \frac{WT(t) - WT(t+1)}{\tan(\alpha)} \qquad [\text{m}]. \tag{56}$$

This leads to an areal change of the pond area,

$$A(t+1) = \pi\left(\sqrt{\frac{A(t)}{\pi}} + \Delta_R\right)^2 \qquad [\text{m}^2] \tag{57}$$

Since the vegetated part of the pond surrounds the open-water part, the area of the open-water part only changes after the whole vegetated area is above the water table. Thus, we can compute the new areas of the two pond fractions in the following way:

$$A_v(t+1) = \max\{0, A_v(t) + A(t+1) - A(t)\}, \qquad [\text{m}^2], \tag{58}$$

$$A_o(t+1) = A(t+1) - A_v(t+1) \qquad [\text{m}^2]. \tag{59}$$

Now we compute the changes in the mean water depths for different cases.

Case $\mathbf{A_o(t+1) = A_o(t) > 0}$

In this case, the water table change of the open-water part is proportional the the water table change of the whole pond,

$$\overline{h_o(t+1)} = \overline{h_o(t)} + WT(t) - WT(t+1) \qquad [\text{m}]. \tag{60}$$

If $A_v(t+1) > 0$ m, then we can recompute the volume of the vegetated pond fraction in time step $t+1$ as a hollow, truncated cone (see eq. 46) and divide by the updated area $A_v(t+1)$ (eq. 47).

Case $\mathbf{A_o(t+1) \neq A_o(t)}$ and $\mathbf{A_o(t+1) > 0}$

If the volume of the open-water part changes, we compute the total volume changes of the pond,

$$\Delta_V = \pi \frac{\tan(\alpha)}{3} \left(R(t+1)^3 - R(t)^3 \right) \qquad [\text{m}^3]. \tag{61}$$

If the water table fell below the vegetated part of the pond, then $\overline{h_v(t+1)} = 0$ and we can compute the new mean depths of the open-water part using the volume change,

$$\overline{h_o(t+1)} = \frac{A_o(t) \cdot \overline{h_o(t)} + \Delta_V}{A_o(t+1)} \qquad [\text{m}]. \tag{62}$$

If both the vegetated and open-water areas changed, we could compute the volume change over the vegetated part as a hollow, truncated cone. The cone spans from the largest extent of the pond in the two time steps to the largest extend of the open-water fraction of the pond, because this is where the vegetated part starts,

$$R_{\min} = \sqrt{\frac{\max\{A_o(t), A_o(t+1)\}}{\pi}} \qquad [\text{m}], \tag{63}$$

$$R^{\max} = \sqrt{\frac{\max\{A(t), A(t+1)\}}{\pi}} \qquad [\text{m}], \tag{64}$$

$$\Delta_{V_v} = \operatorname{sgn}(A(t+1) - A(t)) \cdot \pi \frac{\tan(\alpha)}{3}, \tag{65}$$

$$\cdot (R^3_{\max} - 3R_{\max} \cdot R^2_{\min} + 2R^3_{\min}) \qquad [\text{m}^3]. \tag{66}$$

The mean depth can then be computed as the volume of each part in the new time step divided by the area,

$$\overline{h_v(t+1)} = \frac{\overline{h_v(t)} \cdot A_v(t) + \Delta_{V_v}}{A_v(t+1)} \qquad [\text{m}], \tag{67}$$

$$\overline{h_o(t+1)} = \frac{\overline{h_o(t)} \cdot A_o(t) - \Delta_{V_v} + \Delta_V}{A_o(t+1)} \qquad [\text{m}]. \tag{68}$$

Case $\mathbf{A_o(t) = 0}$

If the whole pond is vegetated, all changes in water depths translate to changes in the vegetated pond fraction. We again compute the volume change as in eq. (61) and compute the new mean depth analogously to Eq. (62).

Finally, we now have computed the new $\overline{h_{o/v}}(t+1)$, the area of the whole pond, and the area of the vegetated and overgrown part of the pond, as well as the new water table.

Supplement 3: Figures

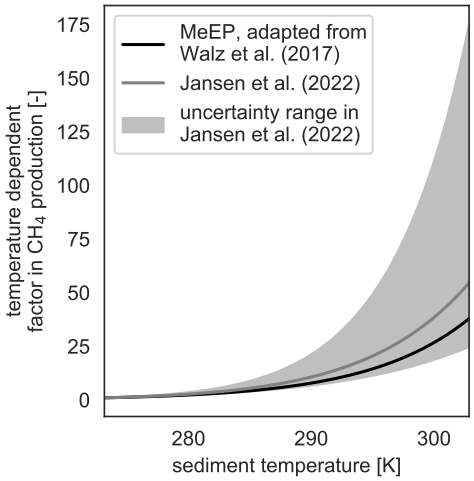

Figure S3: We compare the temperature dependent term in the Arrhenius-type function used by Jansen et al. (2022) in their global synthesis of methane production at lakes bottoms to local measurements of the temperature dependence at our study site using a q_{10} function (Walz et al., 2017). Jansen et al. (2022) provides an uncertainty range in their synthesis (grey shaded area) on top of the average value (grey line). Our local estimate (black line) falls within this uncertainty for the temperature range of pond sediments in our simulations.

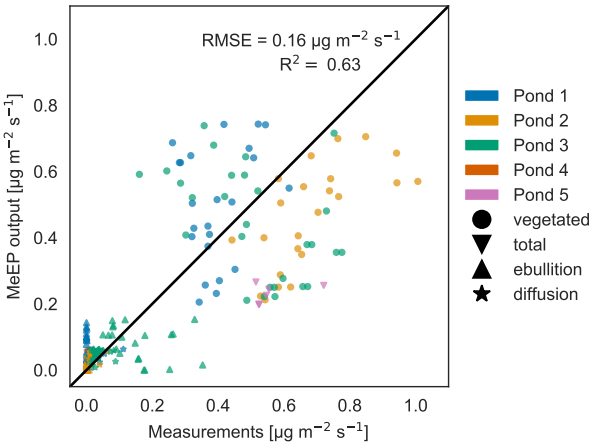

Figure S4: Measured versus tuned modeled methane emissions using a q_{10} of 2. Comparison of measured (x-axis) and modeled (y-axis) methane fluxes for the five ponds measured by Knoblauch et al. (2015) (color code). The fluxes are broken down into different pathways (ebullition and diffusion) where possible. Vegetated fluxes are fluxes measured over the overgrown part of the pond.

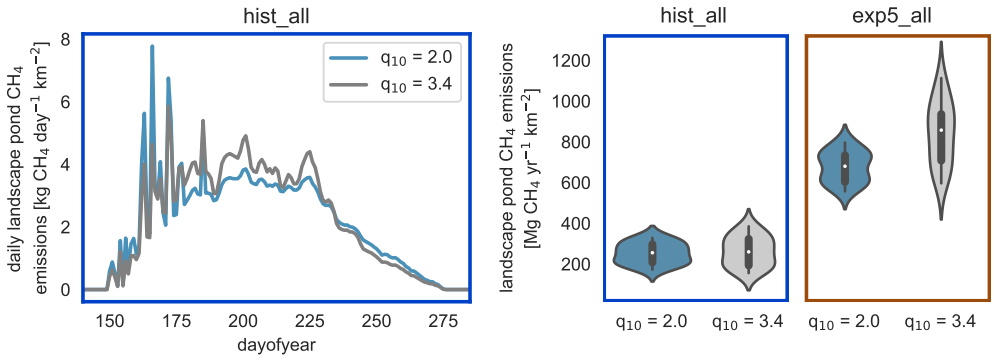

Figure S5: (a) Comparison between the annual cycle of MeEP tuned once with an q_{10} of 2 (blue line) and once with an q_{10} of 3.4 in accordance with Walz et al. (2017) (grey line). The seasonal development and absolute magnitude of the landscape pond CH_4 emissions is very similar in both cases. (b) Comparison of distribution of total annual emissions of MeEP tuned once with an q_{10} of 2 (blue) and once with an q_{10} of 3.4 (grey) for the hist_all (blue frame, left) and exp5_all simulation.

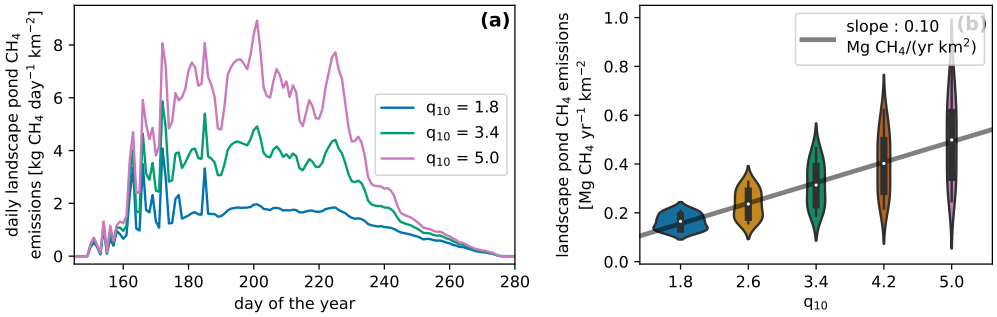

Figure S6: (a) Comparison between the annual cycle of MeEP tuned once with an q_{10} of $1.8, 3.4$ and 5.0 (blue line, green line and pink line, respectively), the estimated mean plus/minus standard deviation of the local q_{10} by Walz et al. (2017) (3.4 ± 1.6). The same tuning (using an q_{10} of 3.4 was used for all three simulations. (b) Comparison of distribution of total annual emissions of MeEP with changes in q_{10}. As q_{10} increases, the average annual emissions and the spread in average annual emissions increase.

References

C. G. Andresen, M. J. Lara, C. E. Tweedie, and V. L. Lougheed. Rising plant-mediated methane emissions from arctic wetlands. *Global Change Biology*, 23(3):1128–1139, 2017. ISSN 1354-1013. doi: https://doi.org/10.1111/gcb.13469.

J. R. M. Arah and K. D. Stephen. A model of the processes leading to methane emission from peatland. *Atmospheric Environment*, 32(19):3257–3264, 1998. ISSN 1352-2310. doi: 10.1016/S1352-2310(98)00052-1.

N. M. Bazhin. Gas transport in a residual layer of a water basin. *Chemosphere - Global Change Science*, 3(1): 33–40, 2001. ISSN 1465-9972. doi: 10.1016/S1465-9972(00)00041-6.

F. Bouchard, I. Laurion, V. Prèskienis, D. Fortier, X. Xu, and M. J. Whiticar. Modern to millennium-old greenhouse gases emitted from ponds and lakes of the eastern canadian arctic (bylot island, nunavut). *Biogeosciences*, 12(23):7279–7298, 2015. ISSN 1726-4189. doi: 10.5194/bg-12-7279-2015.

J. F. Dean, O. H. Meisel, M. Martyn Rosco, L. B. Marchesini, M. H. Garnett, H. Lenderink, R. van Logtestijn, A. V. Borges, S. Bouillon, T. Lambert, T. Röckmann, T. Maximov, R. Petrov, S. Karsanaev, R. Aerts, J. van Huissteden, J. E. Vonk, and A. J. Dolman. East siberian arctic inland waters emit mostly contemporary carbon. *Nature Communications*, 11(1):1627, 2020. ISSN 2041-1723. doi: 10.1038/s41467-020-15511-6.

H. Gao, Q. Tang, X. Shi, C. Zhu, T. Bohn, F. Su, M. Pan, J. Sheffield, D. Lettenmaier, and E. Wood. *Water budget record from Variable Infiltration Capacity (VIC) model*, pages 120–173. 2010.

J. J. Heiskanen, I. Mammarella, S. Haapanala, J. Pumpanen, T. Vesala, S. Macintyre, and A. Ojala. Effects of cooling and internal wave motions on gas transfer coefficients in a boreal lake. *Tellus Series B-Chemical and Physical Meteorology*, 66, 2014. ISSN 1600-0889. doi: 10.3402/tellusb.v66.22827.

M. Helbig, J. Boike, M. Langer, P. Schreiber, B. R. K. Runkle, and L. Kutzbach. Spatial and seasonal variability of polygonal tundra water balance: Lena river delta, northern siberia (russia). *Hydrogeology Journal*, 21(1): 133–147, 2013. ISSN 1435-0157. doi: 10.1007/s10040-012-0933-4.

W. Huang, Z. Zhang, Z. Li, M. Leppäranta, L. Arvola, S. Song, J. Huotari, and Z. Lin. Under-ice dissolved oxygen and metabolism dynamics in a shallow lake: The critical role of ice and snow. *Water Resources Research*, 57(5):e2020WR027990, 2021. ISSN 0043-1397. doi: 10.1029/2020WR027990.

J. Jansen, R. I. Woolway, B. M. Kraemer, C. Albergel, D. Bastviken, G. A. Weyhenmeyer, R. Marcé, S. Sharma, S. Sobek, L. J. Tranvik, M. Perroud, M. Golub, T. N. Moore, L. Råman Vinnå, S. La Fuente, L. Grant, D. C. Pierson, W. Thiery, and E. Jennings. Global increase in methane production under future warming of lake bottom waters. *Global Change Biology*, 28(18):5427–5440, 2022. doi: https://doi.org/10.1111/gcb.16298.

A. Joabsson and T. R. Christensen. Methane emissions from wetlands and their relationship with vascular plants: an arctic example. *Global Change Biology*, 7(8):919–932, 2001. ISSN 1354-1013. doi: https://doi.org/10.1046/j.1354-1013.2001.00044.x.

C. Knoblauch, O. Spott, S. Evgrafova, L. Kutzbach, and E. M. Pfeiffer. Regulation of methane production, oxidation, and emission by vascular plants and bryophytes in ponds of the northeast siberian polygonal tundra. *Journal of Geophysical Research-Biogeosciences*, 120(12):2525–2541, 2015. ISSN 2169-8953. doi: 10.1002/2015jg003053.

K. Martinez-Cruz, A. Sepulveda-Jauregui, K. Walter Anthony, and F. Thalasso. Geographic and seasonal variation of dissolved methane and aerobic methane oxidation in alaskan lakes. *Biogeosciences*, 12(15):4595–4606, 2015. ISSN 1726-4189. doi: 10.5194/bg-12-4595-2015.

Z. Rehder, A. Zaplavnova, and L. Kutzbach. Identifying drivers behind spatial variability of methane concentrations in east siberian ponds. *Frontiers in Earth Science*, 9(183), 2021. ISSN 2296-6463. doi: 10.3389/feart.2021.617662.

A. F. Sabrekov, B. R. K. Runkle, M. V. Glagolev, I. E. Terentieva, V. M. Stepanenko, O. R. Kotsyurbenko, S. S. Maksyutov, and O. S. Pokrovsky. Variability in methane emissions from west siberia's shallow boreal lakes on a regional scale and its environmental controls. *Biogeosciences*, 14(15):3715–3742, 2017. ISSN 1726-4170. doi: 10.5194/bg-14-3715-2017.

R. Sander. Compilation of henry's law constants (version 4.0) for water as solvent. *Atmospheric Chemistry and Physics*, 15(8):4399–4981, 2015. ISSN 1680-7316. doi: 10.5194/acp-15-4399-2015.

V. M. Stepanenko, E. E. Machul'skaya, M. V. Glagolev, and V. N. Lykossov. Numerical modeling of methane emissions from lakes in the permafrost zone. *Izvestiya Atmospheric and Oceanic Physics*, 47(2):252–264, 2011. ISSN 0001-4338. doi: 10.1134/S0001433811020113.

L. Ström, A. Ekberg, M. Mastepanov, and T. Røjle Christensen. The effect of vascular plants on carbon turnover and methane emissions from a tundra wetland. *Global Change Biology*, 9(8):1185–1192, 2003. ISSN 1354-1013. doi: https://doi.org/10.1046/j.1365-2486.2003.00655.x.

L. Ström, M. Mastepanov, and T. R. Christensen. Species-specific effects of vascular plants on carbon turnover and methane emissions from wetlands. *Biogeochemistry*, 75(1):65–82, 2005. ISSN 1573-515X. doi: 10.1007/s10533-004-6124-1.

J. C. Turner, C. J. Moorberg, A. Wong, K. Shea, M. P. Waldrop, M. R. Turetsky, and R. B. Neumann. Getting to the root of plant-mediated methane emissions and oxidation in a thermokarst bog. *Journal of Geophysical Research: Biogeosciences*, 125(11):e2020JG005825, 2020. ISSN 2169-8953. doi: https://doi.org/10.1029/2020JG005825.

B. P. Walter, M. Heimann, R. D. Shannon, and J. R. White. A process-based model to derive methane emissions from natural wetlands. *Geophysical Research Letters*, 23(25):3731–3734, 1996. ISSN 0094-8276. doi: Doi 10.1029/96gl03577.

B. P. Walter, M. Heimann, and E. Matthews. Modeling modern methane emissions from natural wetlands 1. model description and results. *Journal of Geophysical Research-Atmospheres*, 106(D24):34189–34206, 2001. ISSN 2169-897x. doi: 10.1029/2001JD900165.

K. M. Walter, J. P. Chanton, F. S. Chapin III, E. A. G. Schuur, and S. A. Zimov. Methane production and bubble emissions from arctic lakes: Isotopic implications for source pathways and ages. *Journal of Geophysical Research: Biogeosciences*, 113(G3), 2008. ISSN 0148-0227. doi: https://doi.org/10.1029/2007JG000569.

J. Walz, C. Knoblauch, L. Böhme, and E.-M. Pfeiffer. Regulation of soil organic matter decomposition in permafrost-affected siberian tundra soils - impact of oxygen availability, freezing and thawing, temperature, and labile organic matter. *Soil Biology and Biochemistry*, 110:34–43, 2017. ISSN 0038-0717. doi: https://doi.org/10.1016/j.soilbio.2017.03.001.

R. Wanninkhof. Relationship between wind-speed and gas-exchange over the ocean. *Journal of Geophysical Research-Oceans*, 97(C5):7373–7382, 1992. ISSN 0148-0227. doi: 10.1029/92jc00188.

R. Wanninkhof. Relationship between wind speed and gas exchange over the ocean revisited. *Limnology and Oceanography-Methods*, 12:351–362, 2014. ISSN 1541-5856. doi: 10.4319/lom.2014.12.351.

S. Zubrzycki, L. Kutzbach, G. Grosse, A. Desyatkin, and E. M. Pfeiffer. Organic carbon and total nitrogen stocks in soils of the lena river delta. *Biogeosciences*, 10(6):3507–3524, 2013. ISSN 1726-4189. doi: 10.5194/bg-10-3507-2013.